Cross-shore Structure of Longshore Currents during Duck94

Falk Feddersen[1], R.T. Guza[2], Steve Elgar[3], and
T.H.C Herbers[4]

Abstract

The cross-shore structure of the mean longshore current on a barred beach is investigated with observations from the Duck94 field experiment. Maxima of the hourly-averaged longshore current are most frequently located either slightly inshore of the bar crest or near the shoreline. At low tide the longshore current maxima are located closer to the bar crest, and the current is stronger and narrower than at high tide. The tidal cross-shore displacement of the longshore current maximum is qualitatively consistent with the observed radiation stress, S_{xy}, although the maximum currents are displaced shoreward of the maximum S_{xy} gradients at both high and low tide. This spatial lag suggests that some mechanism (such as wave rollers) delays the transfer of momentum from waves to the mean low. Bathymetric longshore inhomogeneities may also affect the cross-shore structure of the longshore current.

Introduction

Selected observations from the DELILAH field experiment at Duck N.C. suggest that the maximum of the mean longshore current, $\bar{v}$, occurs between the crest of the sand bar and the trough between the bar and the shoreline (Figures 8-11 of *Church and Thornton*, (1993)), and that longshore current variability is coherent with the approximately 1 m semidiurnal tidal fluctuations in water level (*Thornton and Kim*, 1993). However, the generality of these results over the wide range of wave (*Long*, 1996), wind, and bathymetric (e.g. pronounced sandbars and alongshore inhomogeneities (*Lippmann and Holman*, 1990; *Gallagher*, 1996)) conditions observed at Duck is unknown. Here the cross-shore structure of $\bar{v}$ is further explored with observations from the Duck94 field experiment.

[1] Graduate Student, Scripps Institution of Oceanography, 0209, La Jolla Ca,92037-0209, falk@coast.ucsd.edu

[2] Professor, Scripps Institution of Oceanography, 0209, La Jolla Ca, 92037 -0209, rguza@ucsd.edu

[3] Professor, Washington State University, Pullman Wa, 99164-2752, elgar@eecs.wsu.edu

[4] Assistant Professor, Naval Postgraduate School, Monterey Ca, 93943, herbers@zee.oc.nps.navy.mil

Duck94 Observations

The experiment site is located on a long straight barrier island exposed to the Atlantic Ocean. Directional properties of sea and swell (including the wave radiation stresses, S_{xy}) were estimated with data from a 2-dimensional array of 15 bottom-pressure sensors located in 8 m water depth operated by the Field Research Facility (FRF) of the U.S. Army Corps of Engineers (*Long*, 1996). Longshore currents, wave-induced bottom pressures, and the location of the sea floor were observed with colocated bidirectional electromagnetic current meters, pressure sensors, and sonar altimeters (*Gallagher et al.*, 1996) deployed on a cross-shore transect extending 750 m from the shoreline to 8 m water depth (Figure 1). The sensors were sampled at 2 Hz for approximately two months. At each pressure sensor-current meter pair, hourly values of S_{xy} were crudely estimated using linear theory.
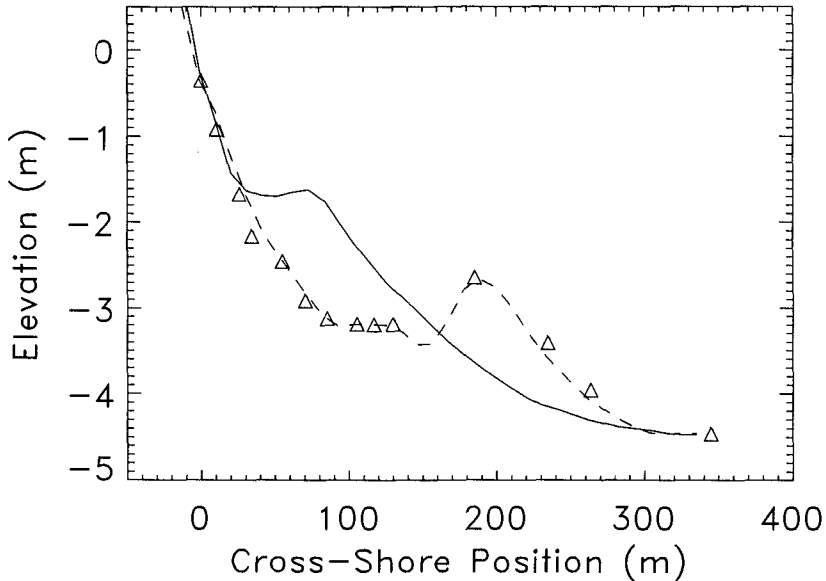

Figure 1. The cross-shore location of current meters (Δ), and measured bathymetry relative to sea level on August 25 (solid line) and October 26 (dashed line). An additional current meter at cross-shore location 749 m in 8 m water depth is not shown.

Conditions during Duck94 are shown in Figure 2. In 8 m water depth, the significant wave height (H_{sig}) ranged between 0.2 m to 4 m and the mean wave angle between $\pm 50^{\circ}$, so that the total (e.g. frequency-integrated) incident wave radiation stress S_{xy}/ρ (where ρ is the water density) in 8 m depth ranged from -0.7 to 0.5 m³/s² (figures 2a-c). The mean (e.g. centroidal) wave frequency ranged from about 0.08 to 0.2 Hz (not shown). Maximum mean longshore currents (in each hour-long record, $\bar{v}_{max}$) ranged from 0.1 to 1.4 m/s (Figure 2d). The bar crest, originally located 80 m from the mean shoreline, gradually migrated 120 m offshore (Figure 2e, after *Gallagher*, 1996). Fluctuations in mean water level were about 1 m at spring tide. The slope of the beach foreshore is about 1/10 (Figure 1), so tidal fuctuations in the location of the mean shoreline are about 10 m. Tidal currents in depths less than 8 m are less than 0.03 m/s (S. Lentz, personal communication 1996).

Results

The sand bar is expected to strongly effect the longshore current, so a normalized cross-shore coordinate is defined as,

$$x' = \frac{x - x_{02}}{x_{bar} - x_{02}}$$

where x is the cross-shore coordinate, x_{bar} is the cross-shore location of the bar crest, and x_{02} is the cross-shore location of the most nearshore sensor uv02. The distance from sensor uv02 to the mean shoreline was typically less than 10 m. Depths at uv02 ($x' = 0$) ranged from about 0.2 to 1.2 m. In this coordinate system, the bar crest is always located at $x' = 1$, but the location of the trough is not constant because of variability in the shape of the cross-shore seafloor profile (e.g. Figure 1).

The location of the longshore current maximum, $\bar{v}_{max}$, is broadly distributed and roughly bimodal in the normalized coordinate system (1) (Figure 3, after *Gallagher*, 1996). Maxima most often occur either slightly inshore of the bar crest ($0.65 \leq x' \leq 1.2$) or near the shoreline ($x' < 0.3$). Rarely does $\bar{v}_{max}$ occur seaward of the bar crest, even when large waves were breaking well seaward of the bar ($x' > 2$). The few maxima located well seaward of the bar crest typically are weak ($\bar{v}_{max} \sim 0.3$ - 0.4 m/s) and approximately correspond to times of strong buoyancy driven flows (Rennie and Largier, personal communication 1996). The stronger longshore currents ($\bar{v}_{max} > 0.8$ m/s) are associated with large offshore S_{xy} (Figures 2c and 2d) and occur near the bar crest ($0.65 < x' < 1.2$). Weaker maxima (0.25 - 0.7 m/s) occur typically near the shoreline ($0 < x' < 0.3$) or near the bar crest, with few maxima in the region in between. Many of the larger $\bar{v}_{max}$ (0.4 - 0.6 m/s) in the region $0 < x' < 0.3$ occur after the sandbar migrated far offshore in mid-October (Figure 2e).
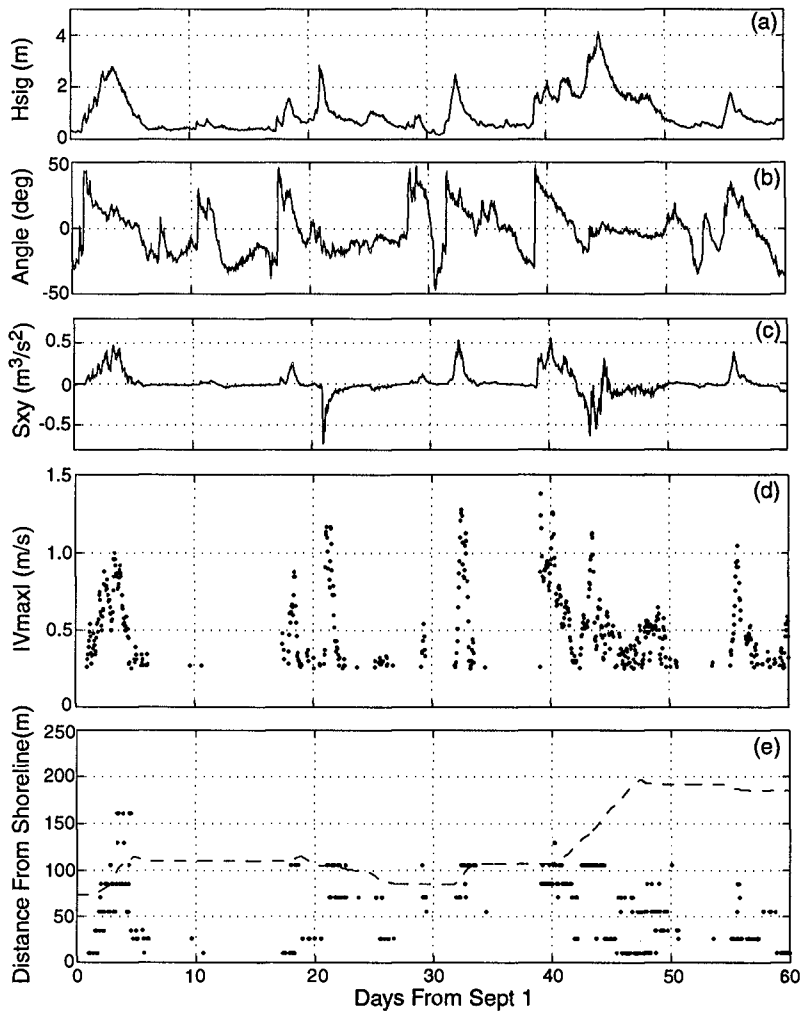
Figure 2. Hourly values of (a) significant wave height H_{sig} in 8 m depth (b) deviation of the mean incident wave angle from shore normal (positive angles correspond to waves from the northern quadrant) (c) S_{xy}/ρ in 8 m depth (d) maximum hour-averaged longshore current $\overline{V}_{max}$ (e) bar crest location (dashed) and the cross-shore location of $\overline{V}_{max}$. $\overline{V}_{max}$ is plotted only if there were at least five active current meters and $\overline{V}_{max} \geq 0.25$ m/s. Out of 1464 possible values, 572 hourly maxima pass these criteria. The few maxima occurring more than 250 m from shore are not shown in (e).
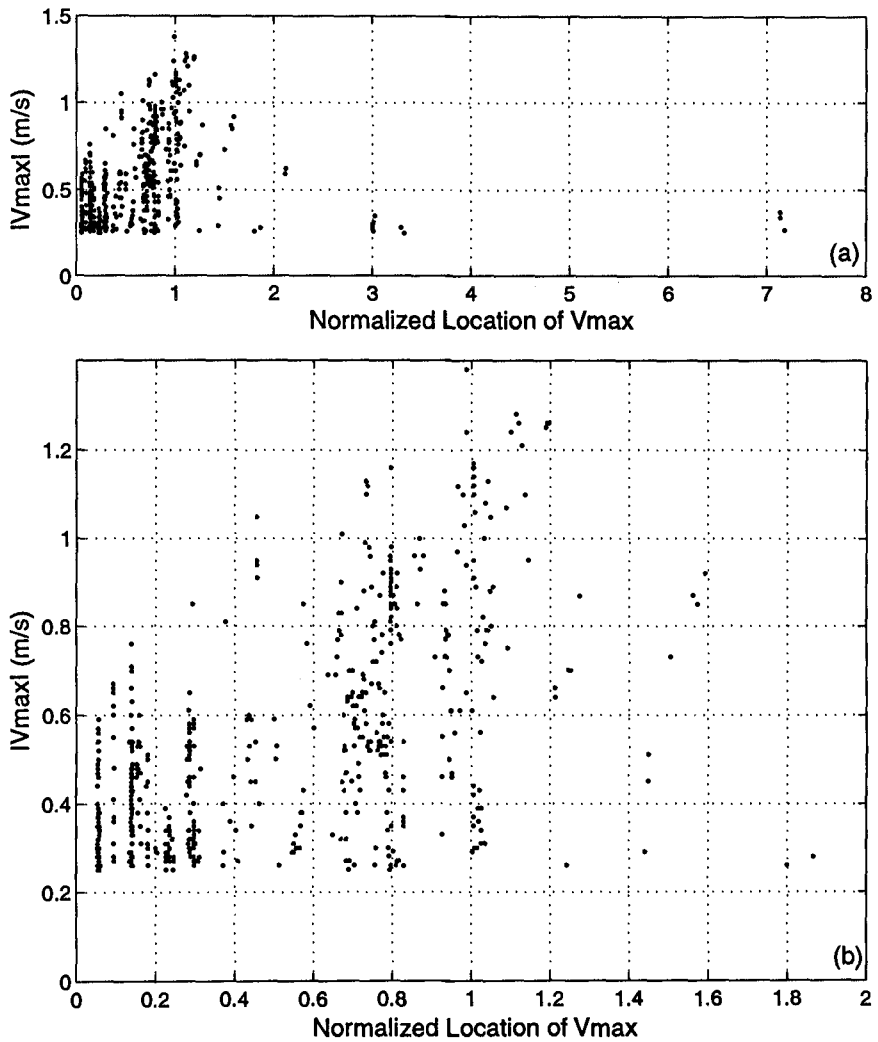
Figure 3. Magnitude of the maximum of the hourly averaged longshore current in normalized cross-shore coordinate, x' (1). the upper panel shows the entire cross-shore region. The region $0 < x' < 2$ is enlarged in the lower panel.

Tides dominate the variability of the local water depth, and thus affect wave shoaling, breaking, and the longshore current. When $\bar{v}_{max}$ is near the bar crest ($0.65 \leq x' \leq 1.2$), the location of $\bar{v}_{max}$ is tidally modulated (Figure 4). At high tide, $\bar{v}_{max}$ is rarely located seaward of $x' = 0.8$, whereas at low tide $\bar{v}_{max}$ is near $x' = 1$. Tidal effects on the location of $\bar{v}_{max}$ are smaller when $\bar{v}_{max}$ is near the shoreline ($x' < 0.3$). Tidal differences in the cross-shore structure of $\bar{v}$ are further illustrated in Figure 5. The current profiles at low tide exhibit a number of similar features; $\bar{v}_{max}$ is located close to $x' = 1$, and the current falls off rapidly shoreward of the maximum. Close to the beach, $\bar{v}$ is approximately 1/4 of $\bar{v}_{max}$. In contrast, at high tide $\bar{v}_{max}$ is farther shoreward (around $x' = 0.7$, consistent with Figure 4) and weaker. The current profile is broader, and near the shoreline $\bar{v}$ is about 1/2-2/3 of $\bar{v}_{max}$. The observed $\bar{v}$ tidal variation is consistent with the phase relationships between $\bar{v}$ and sea-level at tidal frequencies found by *Thornton and Kim* (1993). Wave-breaking induced gradients in significant wave heights are greater during low tide than high tide ($0.8 < x' < 1.5$ in Figure 6), resulting in smaller waves shoreward of the sandbar at low tide ($H_{sig} \sim 0.7$ m) relative to high tide ($H_{sig} \sim 1.0$ m).

The differences within the low (Figure 5a) and high (Figure 5b) tide cross-shore structure of $\bar{v}$ are primarily owing to differences in the conditions over the two days spanned by the observations. The bar was relatively stationary moving 7 m, H_{sig} in 8 m depth ranged from 1 to 2 m (Figure 6), the mean incident wave angle from 15 to 45 degrees, and S_{xy}/ρ from 0.2 to 0.5 m^3/s^2. Similar qualitative features in the tidal variation of $\bar{v}$ were observed at other times when the longshore current was strong for several tidal cycles (e.g. Sept 2-5 and Oct 10-16).

The modeled tidal variation of H_{sig} and $\bar{v}$, for waves and bathymetry representative of Figures 5 and 6, are shown in Figure 7. The wave heights are modeled using *Church and Thornton* (1993), with free model parameters selected to best fit the observed wave heights. The qualitative features of the observed H_{sig} distributions (Figure 6) are reproduced by the model (Figure 7a), except close to the shoreline. The longshore current predictions are made using the modeled H_{sig} variation and observed (in 8 m depth) directional wave properties in the *Thornton and Guza* (1986) longshore current model. A drag coefficient of 0.015 results in similar magnitudes for the modeled (Figure 7b) and observed (Figure 5) currents. Similar to previous results (e.g. *Church and Thornton*, 1993 and others), the modeled longshore currents have the familiar problem of predicting a flow with two maxima, one seaward of the bar crest and one near the shoreline, with no flow in the bar trough. The modeled low and high tide maxima occur at $x' = 1.25$ and $x' = 1.1$ respectively, farther offshore than observed (Figure 5). In physical units, the displacement of the maximum is about 30 m.
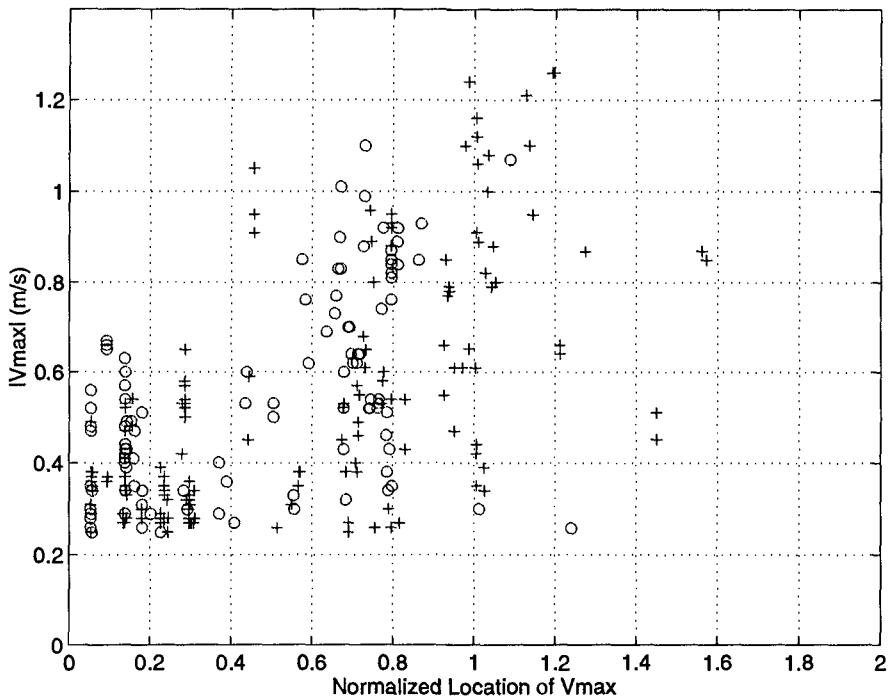
Figure 4. Location and magnitude of $\bar{V}_{max}$, observed within about 1.5 hours of tidal extrema in normalized cross-shore coordinate. There are 157 low tide (+) and 108 high tide (o) values.

Two commonly given reasons (among many) for the model failure are: (1) There may be a spatial lag in the transfer of momentum from the waves to the mean flow, possibly associated with wave rollers (*Svendsen*, 1984; *Dally and Brown*, 1995; and many others). (2) Longshore inhomogeneities in the bathymetry and wave field may result in nonlinear terms or longshore pressure gradient terms in the longshore momentum equation (e.g. *Putrevu et al.*, 1995). Some of the observations are consistent with the lag hypothesis, and there are other examples where alongshore inhomogeneities are likely dominant.

The cross-shore variation of S_{xy} for the successive low and high tide cases (Figure 5 and 6) is shown in Figure 8. At low tide, strong S_{xy} gradients are observed seaward of the bar ($1 \le x' \le 1.5$, Figure 8a), whereas shoreward of the bar crest, S_{xy} is relatively constant. The shoreward displacement of the observed longshore current maxima (Figure 5a) relative to strong S_{xy} gradients (Figure 8a) is consistent with a spatial lag in the transfer of momentum to the mean longshore current. At high tide, the region of strong S_{xy} gradients is

slightly seaward of the bar crest ($0.9 \leq x' \leq 1.25$, Figure 8b), and seaward of the location of $\bar{v}_{max}$ ($x' \sim 0.7$) again indicating a spatial lag in the transfer of momentum to the mean flow. The tidal differences in the cross-shore structure of $\bar{v}$ (i.e. the the broading of $\bar{v}$ at high tide, Figure 5) may be related to tidal variations in the lagging mechanism.
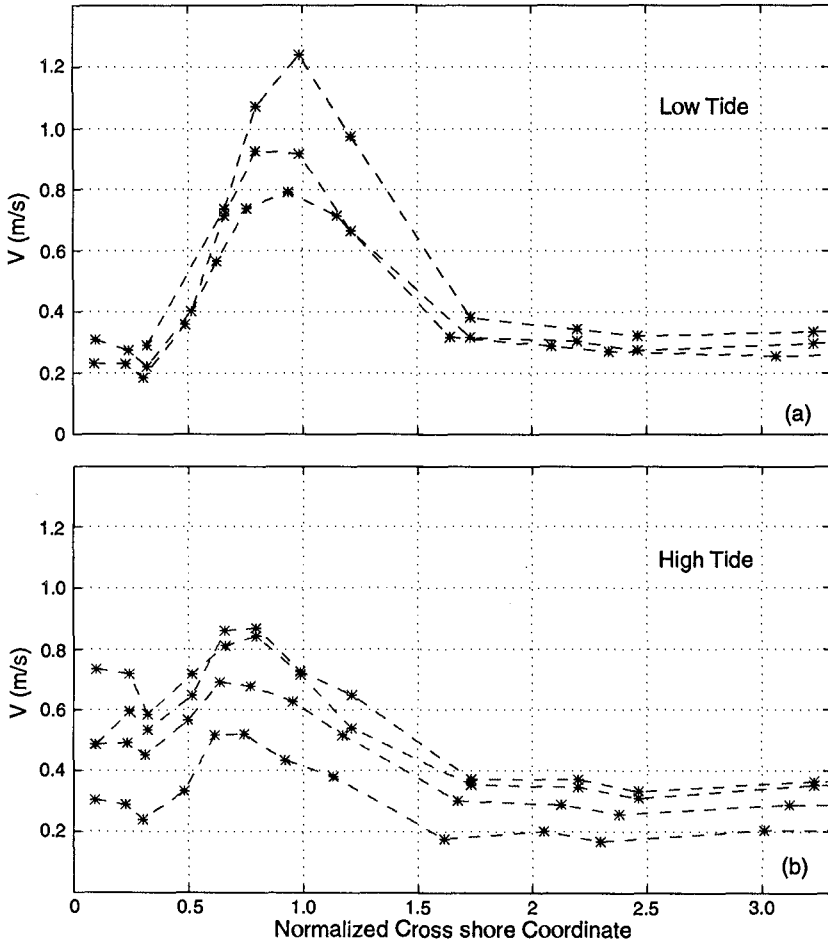

Figure 5. Mean longshore currents in the normalized cross-shore coordinate x' (1) during October 10 and 11. (a) 3 low tides (b) 4 high tides.

Figure 6. Significant wave height in the normalized cross-shore coordinate x' (1) during October 10 and 11. (a) 3 low tides (b) 4 high tides.
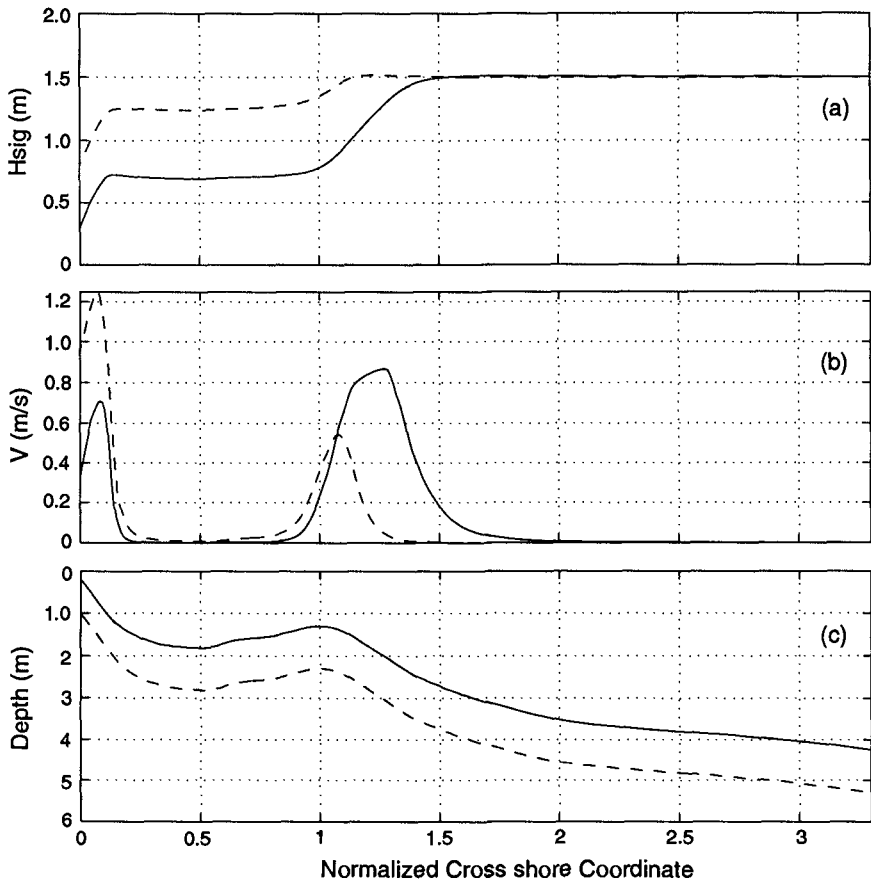
Figure 7. Modeled (a) significant wave heights (b) mean longshore currents (c) model bathymetry in normalized cross-shore coordinate (1). Solid curves represent low tide and dashed curves are high tide. The incident wave parameters are representative of conditions in Figure 5 and 6: $H_{sig} = 1.5$ m and $\theta = 25°$.

An example of longshore currents likely affected by longshore bathymetric inhomogeneities is shown in Figure 9. Although the waves were energetic ($H_{sig} = 3$ m in 8 m depth), they were nearly normally incident (the mean incident wave angle in 8 m depth was 2°) and thus S_{xy} in 8 m depth was small (about 0.1 of S_{xy} with less energetic but more obliquely incident waves in Figure 8). The observations suggest that S_{xy} and S_{xy} gradients are small everywhere (Figure 9b), and that wave breaking began (x >200 m, Figure 9a) far
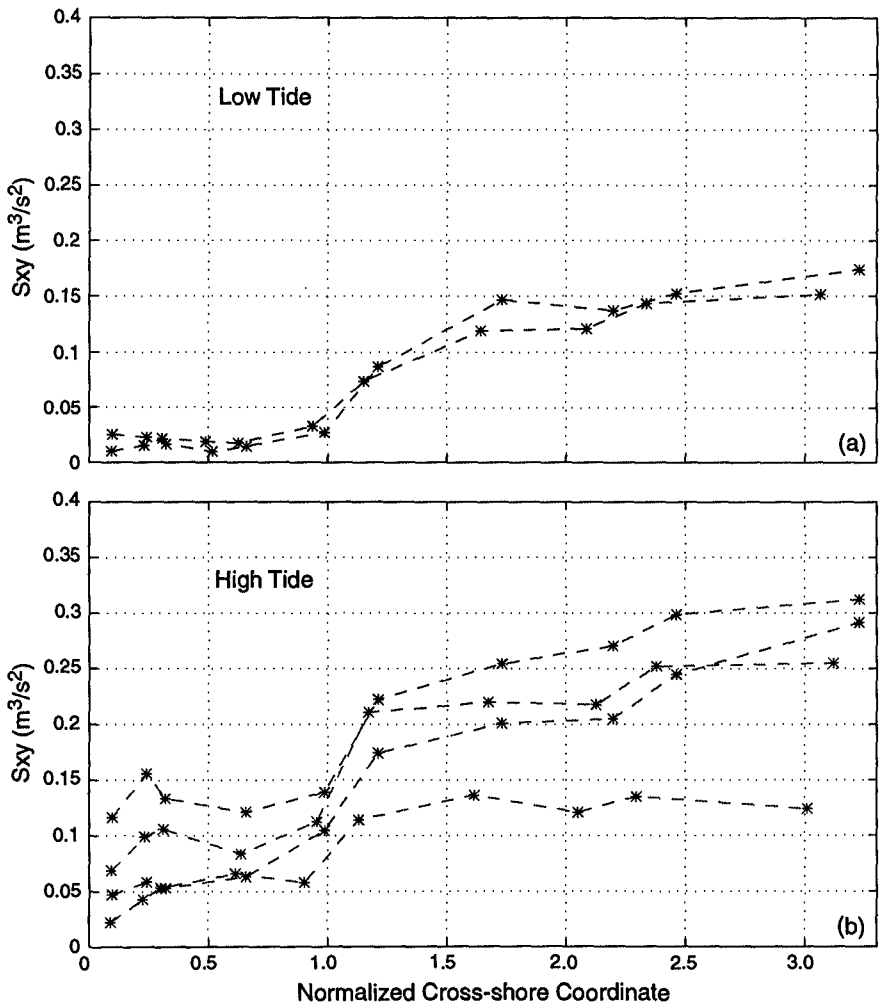
Figure 8. S_{xy}/ρ for the cases (October 10 and 11) shown in Figures 5 and 6 in the normalized cross-shore coordinate x' (1). (a) low tide (b) high tide. The accuracy of S_{xy} estimates is limited because of uncertainties in current meter response and orientation, and because errors in linear theory may be significant in the surfzone. Only two low tide profiles are shown because of unavailable data.

offshore of the location of $\bar{v}_{max}$ ($x \approx 25$ m, Figure 9c). The observed longshore current jet (Figure 9c) near the shoreline is inconsistent with model predictions (based on *Thornton and Guza*, 1986) of negligibly small currents (not shown). Time elapsed video images (R.A. Holman, personal communication, 1996) suggest that the bathymetry was longshore inhomogeneous. Three dimensional bathymetric surveys were not available because of the stormy conditions, however, the first post-storm survey (October 20) did reveal strong longshore inhomogeneity. *Sancho et al.* (1996) demonstrated that this inhomogeneous bathymetry can cause pressure gradients and nonlinear terms to become important in the longshore momentum balance.
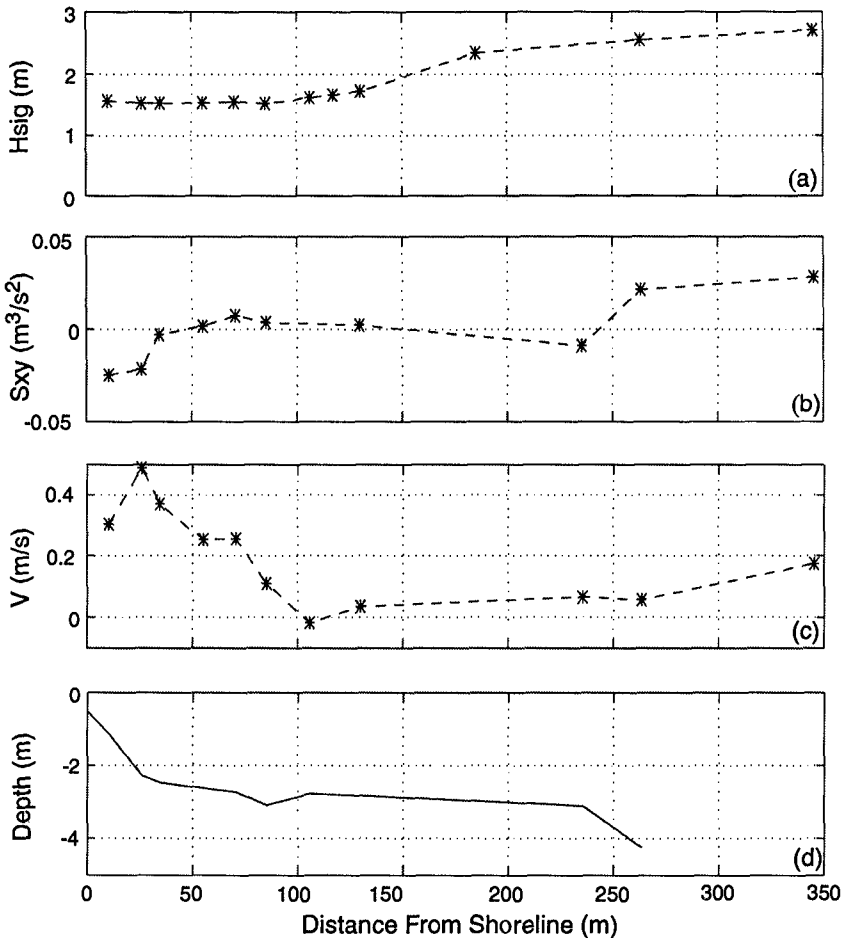
Figure 9. Observed cross-shore variation of (a) significant wave height (b) S_{xy}/ρ (c) longshore current $\bar{v}$ (d) bathymetry on 0500 October 10.

Conclusions

Observations spanning a wide range of bathymetric and wave conditions show that the probability distribution of cross-shore location of longshore current maxima is bimodal. Maxima typically occur near the crest of the sand bar or near the shoreline (Figure 3). At both high and low tide, the observed currents (Figure 5) are qualitatively consistent with the observed S_{xy} (Figure 8), although with a spatial lag, perhaps associated with wave rollers. The 1 m tidal fluctuations in sea level affect the cross-shore structure of the longshore current (Figure 4). At low tide, the current jet is stronger, narrower, and located closer to the bar crest than at high tide (Figure 5). The reason for the tidal changes in the longshore current structure is unknown, however tidal changes in the wave forcing are surely important. Clearly more quantitative work is necessary. The observed variation in the cross-shore structure of the longshore current across a tidal cycle is a robust feature (see also Figure 12 of *Thornton and Kim*, (1993)), and one step in the verification of a roller model would be to reproduce qualitatively the observed tidal variation of the longshore current. Finally, although the magnitude of the effects of longshore bathymetric inhomogeneities is not known, there are cases where they dominate the longshore current (Figure 9).

References

Church, J.C. and E.B. Thornton, Effects of breaking wave induced turbulence within a longshore current model, *Coastal Eng.*, 20, 1-28, 1993.

Dally, W.R. and C.A. Brown, A modeling investigation of the breaking wave roller with application to cross-shore currents, *J. Geophys. Res.*, 100, 24,873-24,883, 1995.

Gallagher, E.L., Observation of sea oor evolution on a natural barred beach. SIO PhD thesis, 62pp. 1996.

Gallagher, E.L., W. Boyd, S. Elgar, R.T. Guza, B. Woodward, Performance of a sonic altimeter in the nearshore, *Marine Geology*, 133, 3, 241-248, 1996.

Lippmann, T.C., and R.A. Holman, The spatial and temporal variability of sand bar morphology, *J. Geophys. Res.*, 95, 11,575-11,590, 1990.

Long, C.E., Index and bulk parameters for frequency-direction spectra measured at CERC Field Research Facility, June 1994 to August 1995, *Miscellaneous Paper CERC-96-6*, U.S. Army Engineer Waterways Experiment Station, Vicksburg, MS, 1996.

Putrevu, U., J. Oltman-Shay, and I.A. Svendsen, Effect of alongshore nonuniformities on longshore current predictions, *J. Geophys. Res.*, 100, 16,119-16,130, 1995.

Sancho, F.E., I.A. Svendsen, A.R. Van Dongeren, and U. Putrevu, Longshore nonuniformities of nearshore currents, *Coastal Dynamics 1995*, 425-436, 1996.

Svendsen, I.A., Wave heights and set-up in a surf zone, *Coastal Eng.*, 8, 303-329, 1984.

Thornton, E.B. and R.T. Guza, Surf zone longshore currents and random waves: field data and models, *J. Phys. Oceanogr.*, 16, 1165-1178, 1986.

Thornton, E.B., and C.S. Kim, Longshore current and wave height modulation at tidal frequency inside the surf zone, *J. Geophys. Res.*, 98, 16,509-16,519, 1993.